Chinese Journal of Electronics
Vol.32, No.4, July 2023

Dual-Band Flexible MIMO Antenna with Self-Isolation Enhancement Structure for Wearable Applications

YANG Lingsheng[1], XIE Yizhang[1], JIA Hongting[2], QU Meixuan[1], LU Zhengyan[1], and LI Yajie[3]

(1. *Nanjing University of Information Science and Technology, Nanjing 210044, China*)

(2. *Kyushu University, 744 Motooka Nishi-Ku, Fukuoka, Japan*)

(3. *Zhongda Hospital Southeast University, Nanjing 210009, China*)

Abstract — A two-element dual-band flexible multi-in multi-out antenna which can be used for wearable applications is proposed in this paper. The antenna consists of two radiating elements fed by coplanar waveguide, and a shielding layer, which are all made of flexible conductive cloth MKKTN260. Each radiating element is composed of two coupled split ring-shaped bending strips. The proposed antenna shows two measured impedance bandwidth (S_{11}<−10 dB) of 2.39–2.48 GHz and 5.72–5.88 GHz, so that it can be used for 2.4 GHz and 5.8 GHz ISM (industrial scientific medical) applications. The two coupled split rings form a self-isolation enhancement structure and can realize polarization diversity at 2.4 GHz band and radiation shielding at 5.8 GHz band, respectively. High isolation (>30 dB) has been achieved for both the bands. Other characteristics for wearable applications like gain, efficiency, specific absorption rate, and bending performances were also studied.

Key words — Flexible antenna, Shielding layer, Coplanar waveguide, Mult-in multi-out, Wearable.

I. Introduction

Wearable technologies have developed rapidly over the the past decade [1], and there is an increasing demand for wearable equipment in different fields such as emergency rescue, health observation, telemedicine, physical exercise, and satellite applications [2]. As a key component of wearable devices, wearable antennas play an important role in determining the device performances. For wearable antennas, some unique design requirements should be paid attention to:

First, the antenna should be small size, low profile, light weight, and easy to integrate with clothing [3]. Textile antenna is a good candidate for wearable antenna designs. In [4]–[7], several textile antennas mounted on felt or jeans material substrates are reported, they all fulfill these requirements, and are comfort and robust when attached to clothes.

Second, the impact of human body on the antenna should be minimized, and for the sake of safety, the specific absorption rate (SAR) should not exceed the threshold. Many efforts have been done to reduce the mutual influence between the antenna and human body [8]–[14]. Electromagnetic band-gap (EBG) layer formed by different types of unit cell is integrated into the antenna [8]–[10], artificial magnetic conductor (AMC) arrays are used in [11]–[13], and high impedance surface (HIS) is introduced to reduce SAR or eliminate the body loading effect in [14]. All these structures can effectively reduce the radiation from antenna to human body, but it needs much effort to design them, and sometimes increase the footprint of the antenna. In [15], cavity structure is utilized to realize uni-directional radiation, but it slightly costs increment to total profile of the antenna.

Finally, the antenna should maintain high data rate transmission when multipath fading, scattering of electromagnetic waves over the body, and shadowing are caused by human body movements [16]. Wearable antennas adopt multi-in multi-out (MIMO) technology are good candidates [17]–[20]. However, when use multiple antenna elements, due to the highly limited size of the wearable antenna system, it is difficult to reduce

Manuscript Received Aug. 19, 2021; Accepted Aug. 16, 2022. This work was supported by the Projects of Superior Subjects in Universities of Jiangsu Province and the Projects of Intelligent Sensing Reasearch Center of Kunshan & Nanjing University of Information Science and Technology.

 DOI:10.23919/cje.2021.00.293

mutual coupling by increasing the distance between antenna elements. Specially designed decoupling structures are usually placed between or above antenna elements to fulfill this goal [18]–[27]. U-shaped ground stub [18] and meta-structures between elements [19] are used to enhance isolation. And in [21], the proper insertion of an "8" shaped stub between the antenna elements provides the stop band characteristics, and reduces the current flowing on the etched ground to the other port. Two degenerated modes of a circular loop is employed in [22], the proposed antenna can maintain high port-to-port isolation without increasing the size. Serial connected two "I" shaped stubs [23], meander line [24], or truncated funnel-shaped area [25] are applied on the ground respectively to obtain high port isolation between antenna elements. A metasurface composed of pairs of non-uniform cut wires with different lengths [26] and a ceramic superstrate [27] are placed above the antennas, which are just as effective to reduce the mutual coupling. Overall layout design of the MIMO system is also effective in enhancing the isolation. Generally, the antenna elements are placed orthogonally to each other [28]–[30], high isolation can be obtained without any specially designed decoupling structures. This method is simple, but the whole antenna system will generally need a large space.

In this letter, we present a flexible MIMO antenna system for 2.4 GHz and 5.8 GHz ISM bands wearable applications. The MIMO antenna system contains two identical radiating elements, each element composes of two coupled split rings. The inner split ring (ISR) and outer split ring (OSR) form a self-isolation enhancement structure, so the MIMO system can obtain higher than 30dB isolation between antennas without any specially designed decoupling structures. The coplanar waveguide (CPW) feeding structure and the shielding layer make the MIMO system easy to fabricate, effective to achieve enhanced front to back ratio, and reduced SAR while maintaining a low profile.

II. Antenna Design

1. Antenna structure and optimization

The geometry of the MIMO antenna system is depicted in Fig.1. As shown in Fig.1(a), the MIMO antenna system consists of two identical radiating elements, which are mounted symmetrically on the top of a 2-mm thick, low cost felt substrate ($\varepsilon_r = 1.36$, $\tan\delta = 0.02$). Each radiating element consists of two coupled split rings. In Fig.1(b), the inner split rings (green parts in Fig.1(a)) are fed by different coplanar waveguides, respectively. The feeding point is connected to the inner conductor of the coaxial cable, and the grounding point is welded to the outer conductor of the cable. The outer split rings (yellow parts in Fig.1(a)) are coupled fed by the inner split rings, respectively. According to Fig.1(b), the OSR is formed by strips L_4, L_5, L_6, and L_7, while the ISR is formed by strips L_8, L_9, and L_{10}. In Fig.1(c), the bottom of the substrate is covered with a sheet of the metallic layer, designed as the shielding layer structure. This structure makes the antenna need no special design of the reflector to sup-

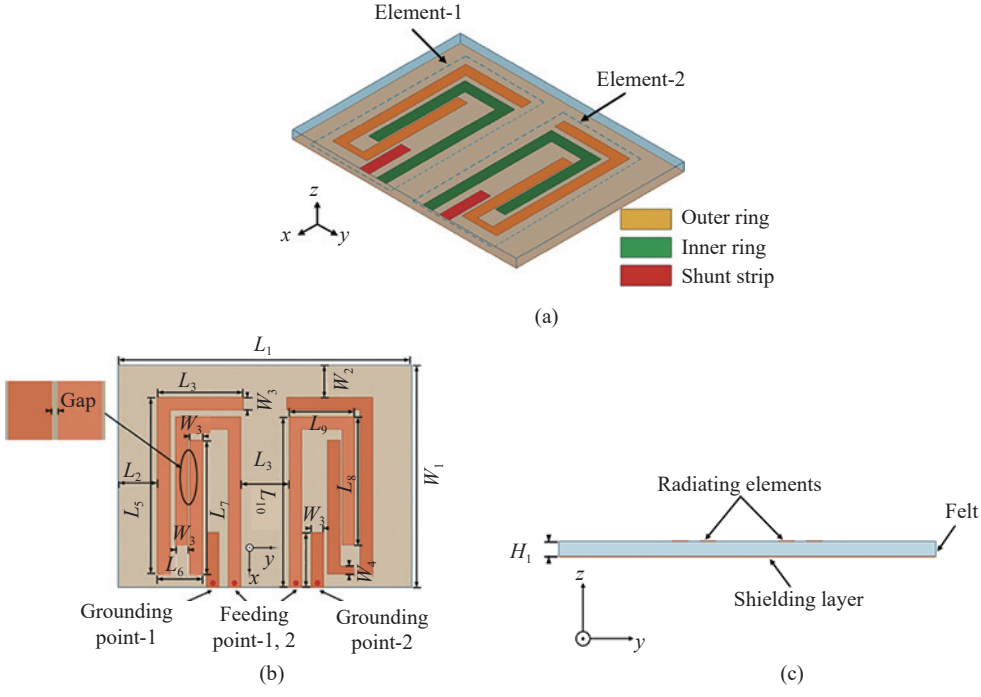

Fig. 1. Geometry of the proposed MIMO antenna. (a) Overall view; (b) Top view; (c) Side view.

press backward radiation, which can simplify the design procedure, and reduce the overall height of the antenna system. At the beginning of the MIMO antenna design, the shielding layer was taken into consideration. The antenna elements and the shielding layer are made of conductive cloth MKKTN260 ($\sigma=8.29\times10^6$ S/m). The total size of the proposed wearable MIMO antenna is 50 mm × 40 mm × 2 mm.

The MIMO antenna is simulated by using HFSS (Ansys, ver.15), and the optimized antenna parameters are displayed in Table 1.

Table 1. Antenna parameters (unit: mm)

L_1	50	L_7	23.7	W_2	5.8
L_2	5.7	L_8	22.6	W_3	2.2
L_3	8.6	L_9	11.7	W_4	1.4
L_4	15.4	L_{10}	30.3	H_1	2
L_5	31.3	L_{11}	9.8	Gap	0.34
L_6	8.1	W_1	40	–	–

The antenna design idea is as follows: In order to make the antenna structure compact, we use half of the CPW structure (feeding strip with only one ground strip) to design the antenna. By combining the direct feeding part of the antenna branch with the coupled feeding part, the low-frequency (or longer) current path of the antenna is formed. At the same time, the path can be "rotated" by bending, thus ensuring high isolation when the spacing between antenna elements is small. It is difficult for the antenna structure to "rotate" in high-frequency band, so it is necessary to add a shielding structure between antenna elements. In this design, the coupling branch will be used to realize the high-frequency current path, and the remaining part of the antenna branch will be used to realize the shielding function. Current paths, discussion of key parameters, and mechanisms for obtaining high isolation are discussed below.

As shown in Fig.2(a), even when the OSR is taken away, the resonance character still exists around 2.4 GHz, but the resonance frequency shifts to a higher frequency. So the 2.4 GHz band is mainly dominated by the ISR, but the resonant frequency is determined by the directly fed ISR structure and the coupled fed OSR structure.

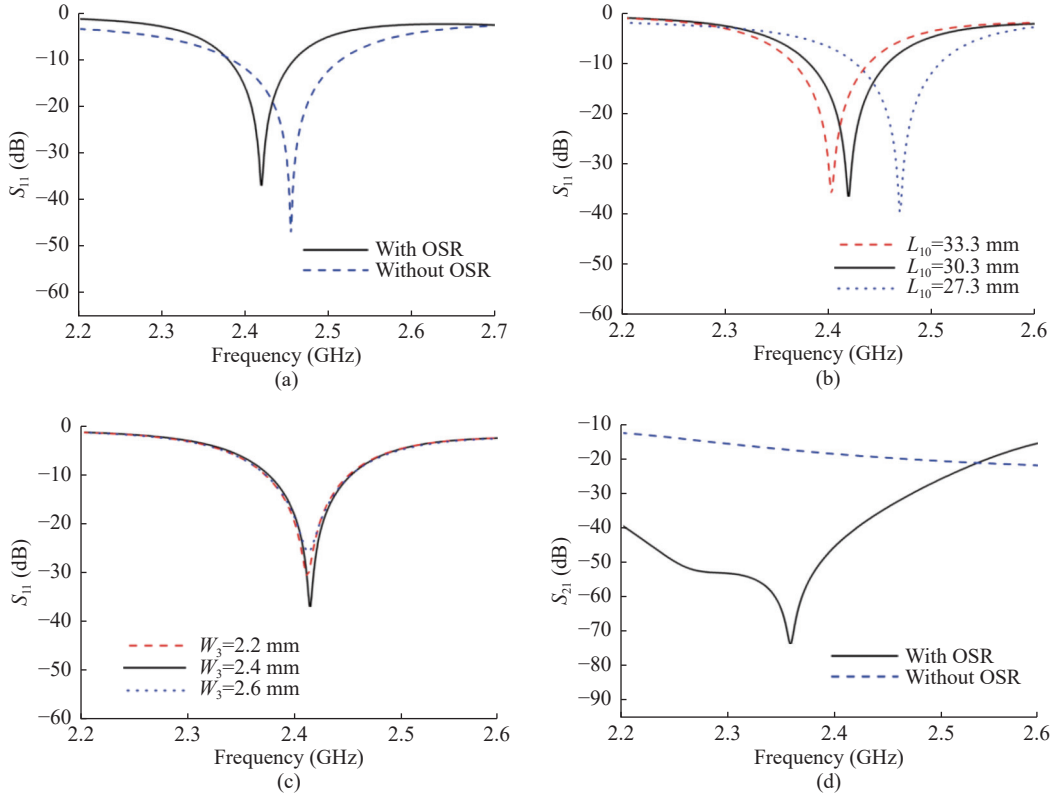

Fig. 2. Simulation of the MIMO antenna at 2.4 GHz. (a) Analysis of S_{11} with change of ring structures; (b) Analysis of S_{11} with the change of L_{10}; (c) Analysis of S_{11} with the change of W_3; (d) Analysis of isolation with the change of ring structures.

In Fig.2(b), as the length of L_{10} increases, the resonant frequency shifts to the lower frequency. Similar variations will appear by changing the length of L_8 or L_9. The total length of the inner split ring is 55 mm, which is approximately half of the wavelength ($\lambda=$ 115 mm) at 2.4 GHz according to formula (1).

$$\lambda = \frac{c}{\sqrt{\varepsilon_{\text{eff}}} f} \tag{1}$$

where c is the speed of light in vacuum, $\varepsilon_{\text{eff}} = \frac{\varepsilon_r+1}{2}$, ε_r is the relative dielectric constant of the felt substrate. As shown in Fig.2(c), there will almost be no influence on both the resonant frequency and the bandwidth for the 2.4 GHz band, even if the width of the strips (W_3) which compose of the inner split ring is changed. The property is very suitable for mass production.

In Fig.2(d), we can see that the OSR structure greatly enhances the isolation between antenna elements.Even the distance between the two elements is only 0.06λ at 2.4 GHz, the isolation is higher than 30 dB. The mechanism can be explained through surface currents distribution characteristics.

Fig.3(a) and (b) depict the excited surface current distribution on Element-2 and Element-1, respectively. We can see that for the two elements, the excited surface current distributes on both the inner and outer split ring structures. Take the surface current distribution on the right element (Element-2) for example, as shown in Fig.3(a), when only Element-2 is excited, Ja represents the total vector sum of J_1, J_2, and J_3; J_b is the total vector sum of J_4, J_7, and J_{10}; while J_5, J_6, J_8, and J_9 constitute the vertically downward total current J_c. The total vector sum currents J_a, J_b, and J_c together form a clockwise rotated current.

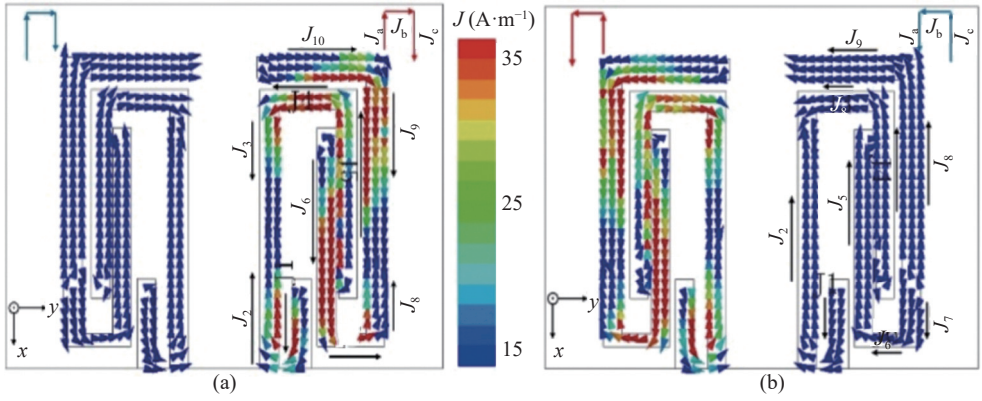

Fig. 3. Surface current distribution at 2.4 GHz. (a) Surface current distribution when only Element-2 is fed; (b) Surface current distribution when only Element-1 is fed.

In Fig.3(b), through the same analytical process, when only the left antenna element (Element-1) is excited, the total vector sum surface currents rotated anticlockwise on the left element (red arrows). Although the strength of the coupled currents on the right antenna element (Element-2) are very low, we still can see that J_1 and J_2 form the vertically downward total current J_a; J_3, J_6, and J_9 form the horizontally leftward total current J_b; meanwhile, J_4, J_5, J_7 and J_8 form the vertically upward total current J_c. So the rotation of the total vector sum coupled currents is also anticlockwise (blue arrows).

In summary, the outer split ring prolongs the current path, and together with the inner split ring, a path with which the surface currents rotate was generated. As shown in Fig.3(a), The excited surface currents on Element-1 and Element-2 rotate in opposite directions, which indicates the polarization of the two elements is just opposite to each other. The high isolation is because the two coupled split rings form a structure that can perform polarization diversity and reduce the coupling between the elements effectively.

In Fig.3(b), we also can see that the rotation between the excited and coupled currents are the same. This is similar to the concept that the signal transmitted by a right-hand circular polarized (RHCP) antenna can be received by the RHCP antenna, while a left-hand circular polarized (LHCP) antenna is hard to or can only receive an extremely low level of the signal. This proves the validity of the proposed coupled split ring structure in forming polarization diversity from another aspect.

Basing on the surface current distribution, we can easily explain how the MIMO antenna works at 5.8 GHz. As plotted in Fig.4, whether for Element-1 or Element-2, the excited currents mainly focus on the vertical strip of the OSR which is close to, and couple fed by the ISR. According to the current direction in Fig.4(a), the antenna element works as a dipole antenna. The length of the current (double-arrow line) is 23.7 mm, about half of the wavelength at 5.8 GHz ($\lambda = 47.6$ mm). Fig.4(a) shows the surface current distribution when only Element-1 is fed, the coupled current on Element-2 is nearly negligible. This is because at 5.8 GHz the ISR works like a radiation shielding structure, and prevents the mutual coupling between the two dipoles, which ensures high isolation.

According to the current distribution shown in

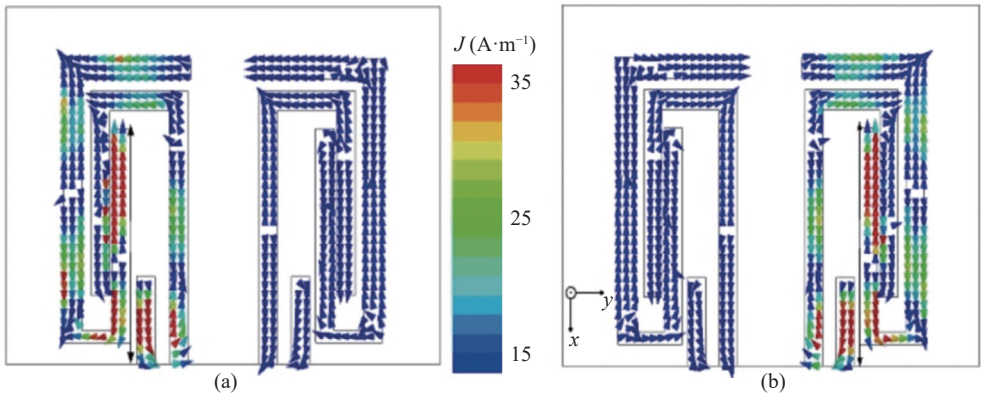

Fig. 4. Surface current distribution at 5.8 GHz. (a) Surface current distribution when only Element-1 is fed; (b) Surface current distribution when only Element-2 is fed.

Fig 4(a) and (b), the radiation on the 5.8 GHz band mainly contributed by the inside arm (L_7) of the outer split ring, the outside arm (L_8) of the inner split ring, and the shunt strip. So the distance (Gap in (Fig.1(b)) between the inside arm of the OSR and the outside arm of the ISR will greatly affect the 5.8 GHz band performances. The distance (L_3) between the two antenna elements is 8.6 mm, which is about 1/6 of the wavelength at 5.8 GHz. However, the simulated isolation is higher than 30 dB throughout the 5.8 GHz ISM band.

Fig.5(a) shows the different performances by the variation of the gap, so that the gap is one of the key design parameters to the 5.8 GHz band. As shown in Fig.5(b), the center frequency of the 5.8 GHz band can be controlled by changing the length of the inside arm (L_7) of the outside ring. The similar phenomenon can be observed by changing the length of the inside arm (L_8) of the inner split ring in Fig.5(c), but its impact is weaker than L_7, so that it can be used as fine adjustment. The width of strips (W_4) is also studied. The changes only have small impact on the impedance matching, and for the sake of clarity, we did not put the results here. The distance (L_3) between the two antenna elements is 8.6 mm, which is about 1/6 of the

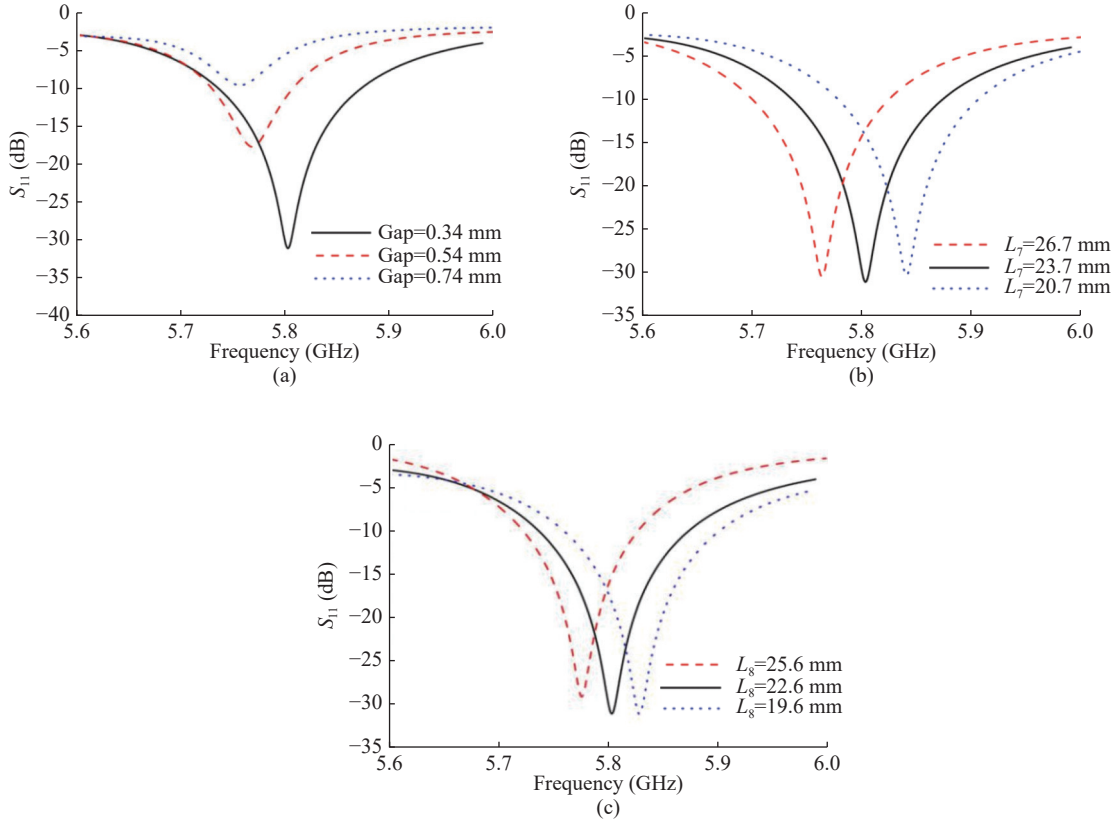

Fig. 5. Parameters study of the MIMO antenna at 5.8 GHz. (a) Analysis of S_{11} with change of the gap; (b) Analysis of S_{11} with the change of L_7; (c) Analysis of S_{11} with the change of L_8.

wavelength at 5.8 GHz. However, the simulated isolation is higher than 30 dB throughout the 5.8 GHz ISM band.

From the above discussion we can see that at 2.4 GHz, the outer split ring (OSR) together with the inner split ring (ISR) realized polarization diversity, while at 5.8 GHz, the ISR performs as a shielding structure. So for both bands, the proposed antenna structure is effective in realizing high isolation between antenna elements, and no extra decoupling designs are needed.

2. SAR values with human tissue model

The value of the specific absorption rate is defined as the power absorbed per unit mass of the tissue.

$$\mathrm{SAR} = \frac{\mathrm{d}}{\mathrm{d}t}\left(\frac{\mathrm{d}W}{\rho \cdot \mathrm{d}V}\right) \ (\mathrm{W/kg}) \tag{2}$$

where W is the energy absorbed by human tissue, ρ is the mass density, and V is the volume of the sample considered. Considering our application scenario, the thickness of the inpatient's clothing is about 2–3 mm, so the MIMO system is placed 3 mm above the three-layer human tissue model (Fig.6) [1]. The model consists of a 2-mm thick skin tissue layer, an 8-mm thick fat tissue layer, and a 23-mm thick muscle tissue layer. The total size of the tissue is $300 \times 300 \times 33$ mm^3. The properties of the human tissues at 2.4 GHz and 5.8 GHz are displayed in Table 2 [31]. The gap between the MIMO antenna and the model is H_0. When the input power is set to 200 mW, the simulation results show that the fat layer has the largest SAR value: 0.024 W/kg and 1.336 W/kg for averaged 1 g body tissue at 2.4 GHz and 5.8 GHz, respectively. The calculated SAR value is less than the IEEE standard of 1.6 W/kg per 1 g tissue [32]. So only by using the combination of half of the CPW-fed structure and the floating ground, safe tissue loading can be realized.

Fig. 6. Side view of the proposed antenna placed on the human tissue model.

Table 2. Human tissue dielectric characteristics [31]

Tissue f	Dry skin		Fat		Muscle	
	ε_r	tanδ	ε_r	tanδ	ε_r	tanδ
2.4 GHz	38.007	0.2949	5.2801	0.1449	52.729	0.2452
5.8 GHz	35.114	0.3336	4.9549	0.1258	48.485	0.3232

III. Antenna Performances

1. Antenna measurements

The MIMO antenna was fabricated and measured with the R&S ZNB20 vector network analyzer when it was placed on the chest of the author and in the free place, respectively (Fig.7).

Fig. 7. Prototype photos. (a) Top view; (b) Bottom view; (c) Placing on the chest.

The simulated and measured S-parameters (Element-1) are shown in Fig.8(a) and (b). It is found that both the measured S-parameters show very good agreement with the simulated results in the entire region. As the antenna is placed on a person's body, the resonant frequencies of the antenna will shift slightly to a higher frequency side comparing in free space. The smaller differences between the simulated and measured results are due to manufacturing errors and the gap between the human tissue model and an actual person's body. It is also found that a person's body slightly causes the deterioration of the isolation between the two radiating elements as shown in Fig.8(b), however, the isolation is still higher than 25 dB in both bands.

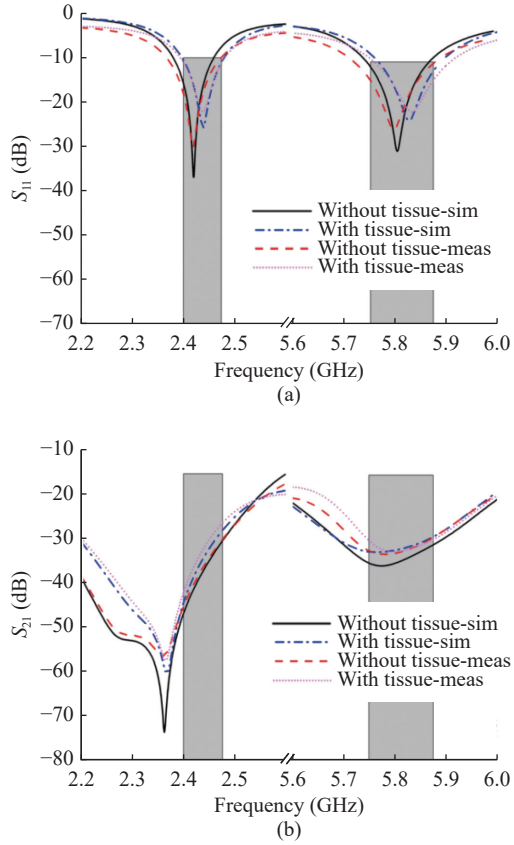

Fig. 8. Simulated and measured S-parameters of the proposed MIMO antenna. (a) S_{11}; (b) S_{21}.

The measured and simulated radiation patterns of the Element-1 are shown in Fig.9. The measured results show very good agreement with the simulated ones. A good front to back ratio (larger than 6 dB) has been obtained with a low profile by introducing a shielding layer structure.

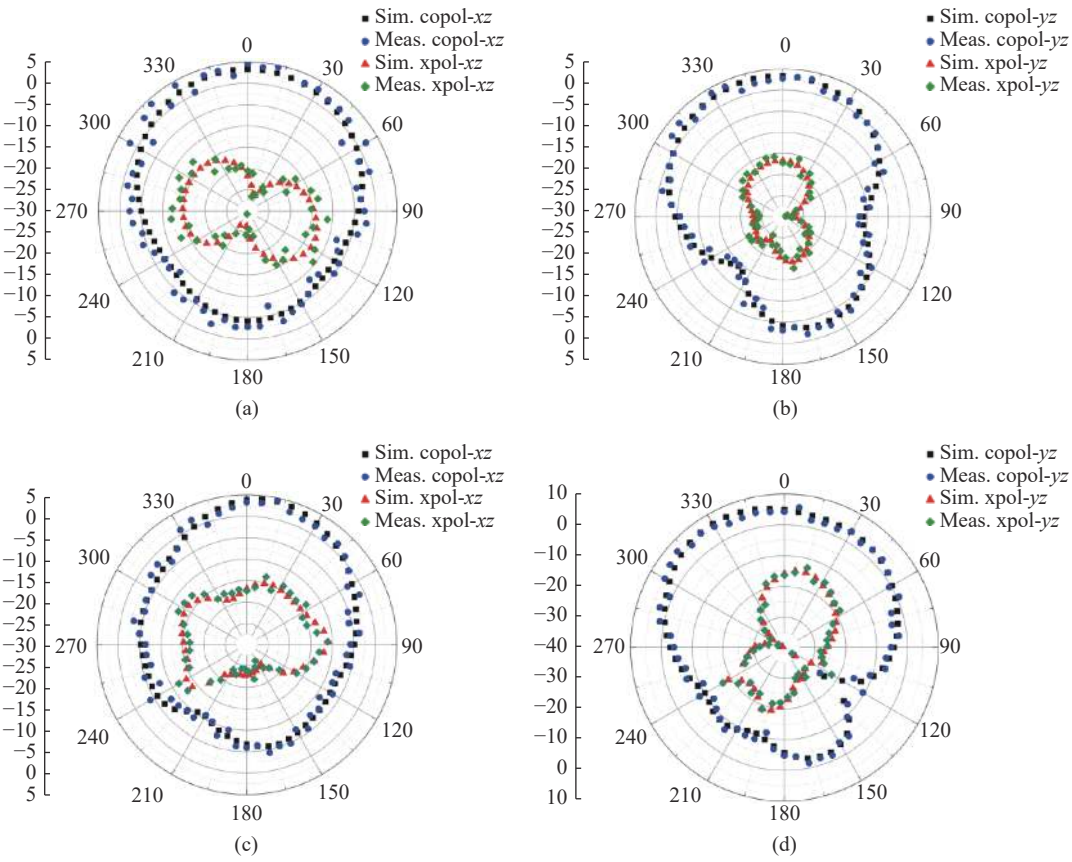

Fig. 9. Simulated and measured radiation patterns of Element-1 at different frequencies. (a) *xoz*@2.4 GHz; (b) *yoz*@2.4 GHz; (c) *xoz*@5.8 GHz; (d) *yoz*@5.8 GHz.

The simulated efficiencies of both the elements 3 mm above the human body model are higher than 30% and 34% for 2.4 GHz and 5.8 GHz respectively. Though the efficiencies are not so high because of the flexible material used [4], and the multi couplings between the inner and the outer ring, but still higher than the antenna proposed in reference [14]. The measured peak gains for both radiating elements at 2.4 GHz and 5.8 GHz bands are higher than 2.4 dBi and 5.2 dBi, respectively. Therefore, stable forward communication can be guaranteed.

2. Bending performances

As the person is moving (such as bending forward or backward), the flexible antenna worn on a person may deform with his body, and varies from the planar state to the bending state. In order to guarantee that the antenna maintains reliable wireless data transmission even in the deformation state, we investigate the antenna performances when the MIMO antenna is bent. The bending state is described using the curvature r, and the smaller the r, the greater the bending. Two different radii (r=50 mm, 1 when normalized to L_1, and r= 28 mm, 0.56 when normalized to L_1) are used for comparison. The isolation S_{21} between the two radiating elements is plotted in Fig.10(a). Although the isolation in the bending state slightly deteriorated compared to its planar state, higher than 25 dB isolation can still be achieved in both bands. As shown in Fig.10(b), the reflection coefficient S_{11} remains almost unchanged in the bending states, but as the bending degree increases (from 57° to 102°), the resonant points shift to lower frequencies.

As shown in Fig.11(a)–(d), the radiation characteristics in the bending state are very close to its planar one, while the forward and the backward radiation are slightly attenuated. The radiation efficiency also decreases slightly by about 1%.

3. MIMO performances

The envelope correlated coefficient (ECC) is commonly used to evaluate the diversity performances of a MIMO system, and for lossy antennas like the proposed wearable antenna, ECC is calculated based on 3D

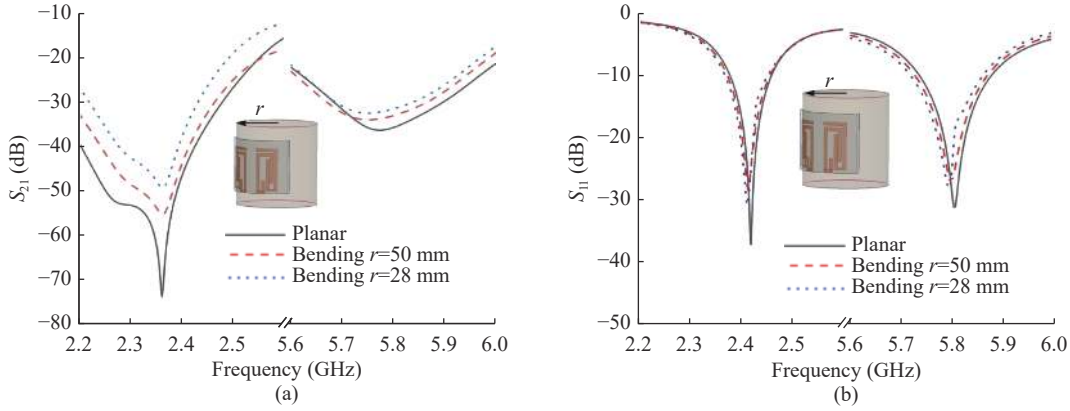

Fig. 10. Antenna performances when in the bending state. (a) Isolation between antenna elements for both status; (b) Impedance matching for both status.

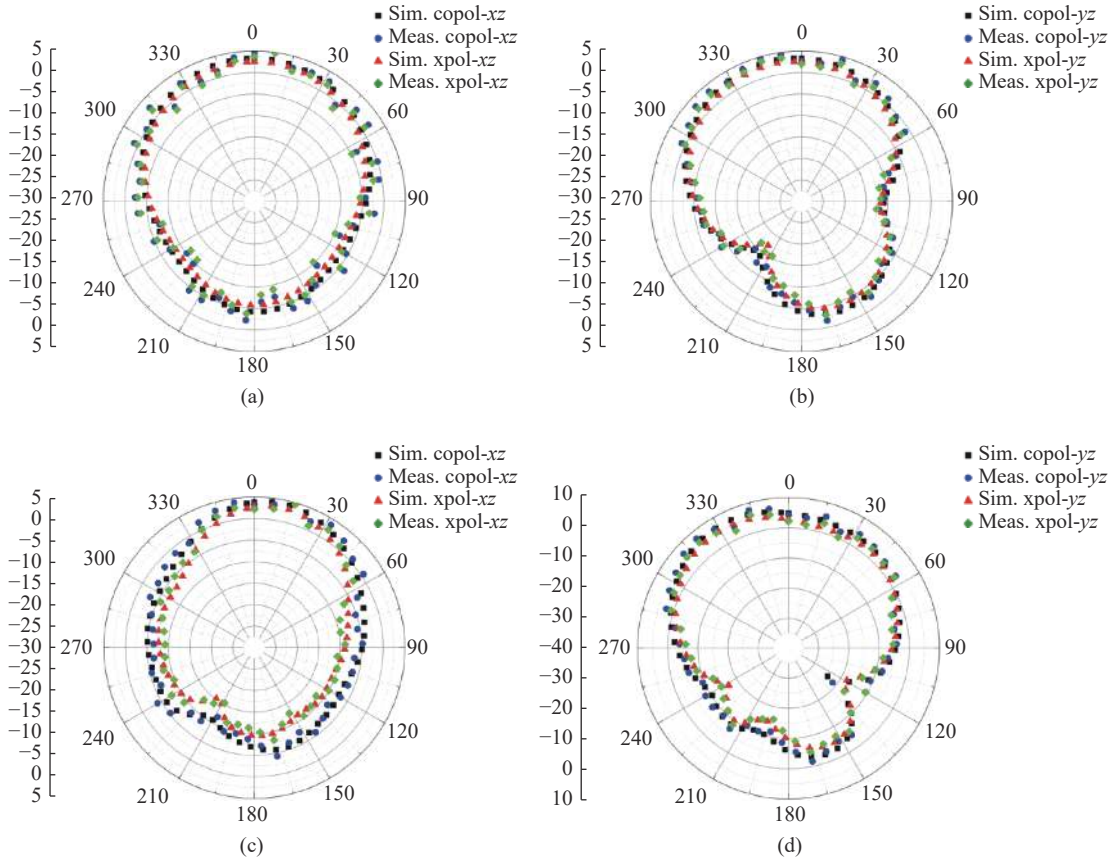

Fig. 11. Comparison of simulated and measured radiation patterns between planar and bending status. (a) xoz@2.4 GHz; (b) yoz@2.4 GHz; (c) xoz@5.8 GHz; (d) yoz@5.8 GHz.

radiation patterns [21]. In the planar state, the ECC of the MIMO antenna system meets the requirements, even in bending status (r=28 mm), for both bands, the simulated and measured results are lower than 0.02 (Fig.12(a)). The simulated value of ECC increases a little more with the increase of the bending angle, but still far below 0.1.

In addition, the diversity gain (DG) is commonly used to measure how the diversity impact on the power transmission of the MIMO antenna system, and can be calculated by

$$\mathrm{DG} = 10 \times \sqrt{1 - |\rho_e|^2} \tag{3}$$

There is little difference in DG between the planar and bending states. As shown in Fig.12(b), for both the simulated and measured DGs, the results are higher than 9.998 dB over the two operation bands. Table 3 shows the comparisons among our design and some recently published wearable MIMO antenna systems. Our

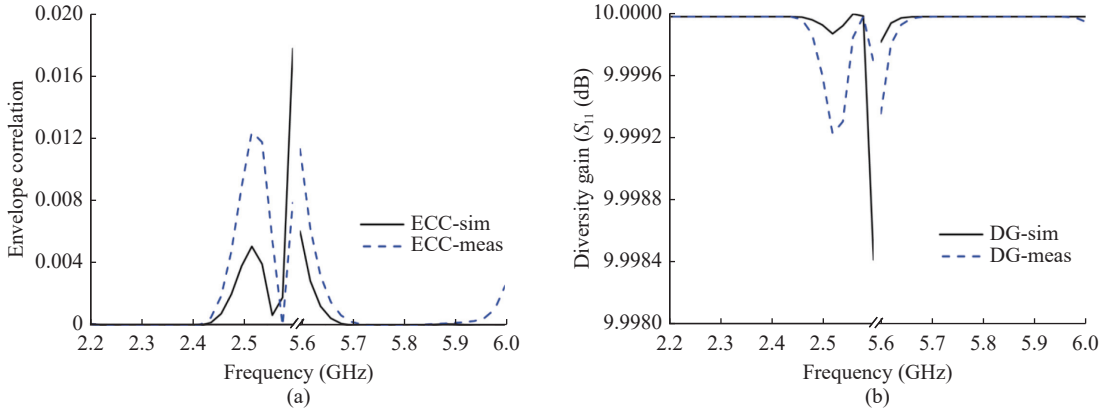

Fig. 12. MIMO parameters for bending status. (a) ECC; (b) DG.

design has a relatively small size, and good isolation performances can be realized through two ISM bands without specially designed decoupling structures or orthogonal arrangement of the antenna elements.

Table 3. Comparisons among antanna systems

Ref.	Dimensions (mm^3)	Operating band (GHz)	Isolation (dB)	Decoupling methods	Element distance (λ)	Gain (dB)
[5]	$101.9 \times 92.3 \times 3$	2.37–2.53 5.16–5.85	18	L^* D^{**}	0.08	2 5.6
[16]	$26 \times 26 \times 0.8$	2.4	25	L^*	0.06	2.4
[17]	$80 \times 50 \times 0.8$	2.4–2.48 5.72–5.87	25	D^{**}	0.1	4.12 4.86
[18]	$28 \times 25 \times 0.5$	2.45	30	D^{**}	> 0.06	0.5
[19]	$190 \times 104 \times 4$	2.16–2.66	40	D^{**}	> 0.1	5.8
[22]	$\pi \times 18^2 \times 7$	2.4–2.49	20	L^*	–	2
[28]	$38.1 \times 38.1 \times 2$	2.4–2.48	15	L^*	–	1.67
Ours	$50 \times 40 \times 2$	2.36–2.48 5.72–5.88	30	Self-structure	0.06	2.4 5.2

Note: L^* = Layout design, D^{**} = Decoupling structures.

IV. Conclusions

In this paper, a flexible dual-band MIMO antenna for wearable applications has been proposed. The antenna can cover the 2.45 GHz and 5.8 GHz bands with a low profile, and is easy to integrate with clothing. The two split rings form a self-isolation enhancement structure and higher than 30 dB isolation can be achieved for both bands, which ensures good MIMO performances of the system. During wearing, the performance of the antenna is robust to the bending caused by position changing or moving.

References

[1] Y. J. Li, Z. Y. Lu, and L. S. Yang, "CPW-fed slot antenna for medical wearable applications," *IEEE Access*, vol.7, pp.42107–42112, 2019.

[2] S. Yan and G. A. E. Vandenbosch, "Radiation pattern-reconfigurable wearable antenna based on metamaterial structure," *IEEE Antennas and Wireless Propagation Letters*, vol.15, pp.1715–1718, 2016.

[3] G. P. Gao, B. Hu, X. L. Tian, *et al.*, "Experimental study of a wearable aperture-coupled patch antenna for wireless body area network," *Microwave and Optical Technology Letters*, vol.59, no.4, pp.761–766, 2017.

[4] P. Van Torre, L. Vallozzi, C. Hertleer, *et al.*, "Indoor off-body wireless MIMO communication with dual polarized textile antennas," *IEEE Transactions on Antennas and Propagation*, vol.59, no.2, pp.631–642, 2011.

[5] S. Yan, P. J. Soh, and G. A. E. Vandenbosch, "Dual-band textile MIMO antenna based on substrate-integrated waveguide (SIW) technology," *IEEE Transactions on Antennas and Propagation*, vol.63, no.11, pp.4640–4647, 2015.

[6] D. C. Xu, X. J. Tian, X. H. Guo, *et al.*, "Design and research of flexible wearable textile antenna based on GNPs/PANI/PDMS composites for 2.45 GHz," *Nanoscience and Nanotechnology Letters*, vol.9, no.4, pp.476–480, 2017.

[7] D. Yamanaka and M. Takahashi, "5.2 GHz band textile antenna for biological information monitoring," *IEICE Transactions on Communications*, vol.J101-B, no.7, pp.584–591, 2018.

[8] S. Z. Zhu and R. Langley, "Dual-band wearable textile antenna on an EBG substrate," *IEEE Transactions on Antennas and Propagation*, vol.57, no.4, pp.926–935, 2009.

[9] A. Iqbal, A. Basir, A. Smida, *et al.*, "Electromagnetic bandgap backed millimeter-wave MIMO antenna for wearable applications," *IEEE Access*, vol.7, pp.111135–111144,

2019.

[10] M. A. B. Abbasi, S. S. Nikolaou, M. A. Antoniades, *et al.*, "Compact EBG-backed planar monopole for BAN wearable applications," *IEEE Transactions on Antennas and Propagation*, vol.65, no.2, pp.453–463, 2017.

[11] H. R. Raad, A. I. Abbosh, H. M. Al-Rizzo, *et al.*, "Flexible and compact AMC based antenna for telemedicine applications," *IEEE Transactions on Antennas and Propagation*, vol.61, no.2, pp.524–531, 2013.

[12] M. El Atrash, M. A. Abdalla, and H. M. Elhennawy, "A wearable dual-band low profile high gain low SAR antenna AMC-backed for WBAN applications," *IEEE Transactions on Antennas and Propagation*, vol.67, no.10, pp.6378–6388, 2019.

[13] Z. H. Jiang, D. E. Brocker, P. E. Sieber, *et al.*, "A compact, low-profile metasurface-enabled antenna for wearable medical body-area network devices," *IEEE Transactions on Antennas and Propagation*, vol.62, no.8, pp.4021–4030, 2014.

[14] Y. S. Chen and T. Y. Ku, "A low-profile wearable antenna using a miniature high impedance surface for smart watch applications," *IEEE Antennas and Wireless Propagation Letters*, vol.15, pp.1144–1147, 2016.

[15] J. Joubert, J. C. Vardaxoglou, W. G. Whittow, *et al.*, "CPW-fed cavity-backed slot radiator loaded with an AMC reflector," *IEEE Transactions on Antennas and Propagation*, vol.60, no.2, pp.735–742, 2012.

[16] I. Elfergani, A. Iqbal, C. Zebiri, *et al.*, "Low-profile and closely spaced four-element MIMO antenna for wireless body area networks," *Electronics*, vol.9, no.2, article no.articleno.258, 2020.

[17] X. M. Ling and R. L. Li, "A novel dual-band MIMO antenna array with low mutual coupling for portable wireless devices," *IEEE Antennas and Wireless Propagation Letters*, vol.10, pp.1039–1042, 2011.

[18] A. Gupta, A. Kansal, and P. Chawla, "Design of a wearable MIMO antenna deployed with an inverted U-shaped ground stub for diversity performance enhancement," *International Journal of Microwave and Wireless Technologies*, vol.13, no.1, pp.76–86, 2021.

[19] A. N. S. S. Agus, T. Sabapathy, M. Jusoh, *et al.*, "Combined RIS and EBG surfaces inspired meta-wearable textile MIMO antenna using Viscose-Wool felt," *Polymers*, vol.14, no.10, article no.articleno.1989, 2022.

[20] X. Y. LU, S. Venkatesh, H. Saeidi, *et al.*, "Integrated Intelligent Electromagnetic Radiator Design for Future THz Communication: A Review," *Chinese Journal of Electronics*, vol.31, no.3, pp.499–515, 2022.

[21] A. Kumar Biswas, and U. Chakraborty, "Compact wearable MIMO antenna with improved port isolation for ultra-wideband applications," *IET Microwaves, Antennas & Propagation*, vol.13, no.4, pp.498–504, 2019.

[22] D. L. Wen, Y. Hao, M. O. Munoz, *et al.*, "A compact and low-profile MIMO antenna using a miniature circular high-impedance surface for wearable applications," *IEEE Transactions on Antennas and Propagation*, vol.66, no.1, pp.96–104, 2018.

[23] A. K. Biswas and U. Chakraborty, "A compact wide band textile MIMO antenna with very low mutual coupling for wearable applications," *International Journal of RF and Microwave Computer-Aided Engineering*, vol.29, no.8, article no.e21769, 2019.

[24] S. Roy, S. Ghosh, S. S. Pattanayak, *et al.*, "Dual-polarized textile-based two/four element MIMO antenna with improved isolation for dual wideband application," *International Journal of RF and Microwave Computer-Aided Engineering*, vol.30, no.9, article no.e22292, 2020.

[25] A. K. Biswas and U. Chakraborty, "Reconfigurable wide band wearable multiple input multiple output antenna with hanging resonator," *Microwave and Optical Technology Letters*, vol.62, no.3, pp.1352–1359, 2020.

[26] F. Liu, J. Y. Guo, L. Y. Zhao, *et al.*, "Dual-band metasurface-based decoupling method for two closely packed dual-band antennas," *IEEE Transactions on Antennas and Propagation*, vol.68, no.1, pp.552–557, 2020.

[27] F. Liu, J. Y. Guo, L. Y. Zhao, *et al.*, "Ceramic superstrate-based decoupling method for two closely packed antennas with cross-polarization suppression," *IEEE Transactions on Antennas and Propagation*, vol.69, no.3, pp.1751–1756, 2021.

[28] H. Li, S. Sun, B. Wang, *et al.*, "Design of compact single-layer textile MIMO antenna for wearable applications," *IEEE Transactions on Antennas and Propagation*, vol.66, no.6, pp.3136–3141, 2018.

[29] A. Iqbal, A. Smida, A. J. Alazemi, *et al.*, "Wideband circularly polarized MIMO antenna for high data wearable biotelemetric devices," *IEEE Access*, vol.8, pp.17935–17944, 2020.

[30] W. T. Li, Y. Q. Hei, P. M. Grubb, *et al.*, "Compact inkjet-printed flexible MIMO antenna for UWB applications," *IEEE Access*, vol.6, pp.50290–50298, 2018.

[31] D. Andreuccetti, R. Fossi, and C. Petrucci, "Calculation of the dielectric properties of body tissues in the frequency range 10 Hz–100 GHz," Available at: *http://niremf.ifac.cnr.it/tissprop/htmlclie/htmlclie.php*, 1997.

[32] IEEE Std C95.3:2002 (Revision of IEEE Std C95.3:1991), IEEE Recommended Practice for Measurements and Computations of Radio Frequency Electromagnetic Fields With Respect to Human Exposure to Such Fields, 100 kHz–300 GHz.

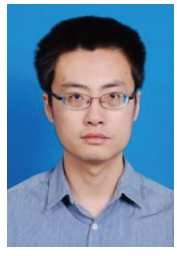

YANG Lingsheng received the B.S. degree in the Department of Communication Engineering, Nanjing University of Science & Technology, China, in 2001, and the M.S. and Ph.D. degrees in the Faculty of Information Science and Electrical Engineering, Kyushu University, Japan, in 2009 and 2012, respectively. (Email: ylsinchina@163.com)

XIE Yizhang recieved the B.S degree in Tianping College of Suzhou University of Science and Technology in 2019. He is currently a graduate student in the Department of Electronies and Information Engineering of Nanjing University of Information Science and Technology, Nanjing, China. His current research interests include wearable antennas and wearable equipment developing.

JIA Hongting received the B.E. degree in electrical engineering from Xidian University, China, in 1987, M.E. and D.E. degrees in communication engineering from Kyushu University, Fukuoka, Japan, in 1996 and 1999, respectively. From 1987 to 1992, he was with the Hebei Semiconductor Research Institute, China. In 1999, he joined the Faculty of Engineering, Nagasaki University, Nagasaki, Japan. In 2001, he joined Kyushu University. His current research interests include RF/microwave circuits, direct/inverse-scattering problems, grating problems, and numerical analysis. He is a Member of the Institute of Electrical, Information, and Communication Engineers, Japan and the Institution of Electrical Engineers, Japan.

QU Meixuan was born in Zhejiang Province, China, in 1999. Now he is an undergraduate student in Electronics & Information Engineering Department, Nanjing University of Information Science and Technology. His research interests include antennas and signal processing.

LU Zhengyan was born in Xuzhou, Jiangsu Province, China, in 1994. He received the B.S.degree in electronics engineering from Nanjing University of Information Science and Technology, in 2016. Now he is a postgraduate student in Electronics & Information Engineering Department, Nanjing University of Information Science and Technology. His research interests include wearable antennas and bioelectromagnetics.

LI Yajie (corresponding author) received the B.S. and M.S. degrees in the School of Medicine, Zhejiang University, China, in 2005 and 2007, respectively. From 2007 to 2012, she worked for the First Affiliated Hospital of Wenzhou Medical University. Since 2012, she has been an Attending Doctor with the Geriatric Department, ZhongDa Hosipital, Southeast University. She is an author of nearly 20 papers. Her research interests include gerontology, internal medicine of digesting, medical engineering, and bioelectromagnetics.
(withlove1982@163.com)